LETTER

doi:10.1038/nature12951

Polarized release of T-cell-receptor-enriched microvesicles at the immunological synapse

Kaushik Choudhuri[1]*, Jaime Llodrá[2]*, Eric W. Roth[3], Jones Tsai[4], Susana Gordo[5,6], Kai W. Wucherpfennig[5,6], Lance C. Kam[4], David L. Stokes[2,7] & Michael L. Dustin[8,9]

The recognition events that mediate adaptive cellular immunity and regulate antibody responses depend on intercellular contacts between T cells and antigen-presenting cells (APCs)[1]. T-cell signalling is initiated at these contacts when surface-expressed T-cell receptors (TCRs) recognize peptide fragments (antigens) of pathogens bound to major histocompatibility complex molecules (pMHC) on APCs. This, along with engagement of adhesion receptors, leads to the formation of a specialized junction between T cells and APCs, known as the immunological synapse[2], which mediates efficient delivery of effector molecules and intercellular signals across the synaptic cleft[3]. T-cell recognition of pMHC and the adhesion ligand intercellular adhesion molecule-1 (ICAM-1) on supported planar bilayers recapitulates the domain organization of the immunological synapse[4,5], which is characterized by central accumulation of TCRs[5], adjacent to a secretory domain[2], both surrounded by an adhesive ring[4,5]. Although accumulation of TCRs at the immunological synapse centre correlates with T-cell function[4], this domain is itself largely devoid of TCR signalling activity[5,6], and is characterized by an unexplained immobilization of TCR–pMHC complexes relative to the highly dynamic immunological synapse periphery[4,5]. Here we show that centrally accumulated TCRs are located on the surface of extracellular microvesicles that bud at the immunological synapse centre. Tumour susceptibility gene 101 (TSG101)[6] sorts TCRs for inclusion in microvesicles, whereas vacuolar protein sorting 4 (VPS4)[7,8] mediates scission of microvesicles from the T-cell plasma membrane. The human immunodeficiency virus polyprotein Gag co-opts this process for budding of virus-like particles. B cells bearing cognate pMHC receive TCRs from T cells and initiate intracellular signals in response to isolated synaptic microvesicles. We conclude that the immunological synapse orchestrates TCR sorting and release in extracellular microvesicles. These microvesicles deliver transcellular signals across antigen-dependent synapses by engaging cognate pMHC on APCs.

The nature of the biophysical environment that governs molecular domain organization at the immunological synapse remains unclear. Confinement of pMHC[4], TCRs[5] and cytoplasm (Supplementary Fig. 1) suggests that a general diffusion barrier separates TCRs and cytoplasm at the immunological synapse centre from the rest of the T cell. To better understand the basis for the observed central confinement of pMHC, TCRs and cytoplasm at the immunological synapse, we investigated $CD4^+$ T-cell immunological synapse formation using high-resolution optical imaging by total internal reflection fluorescence microscopy (TIRFM), integrated with transmission electron microscopy (TEM) and electron tomography.

T cells from TcrAND transgenic mice[9] form TCR microclusters in response to engagement by the cognate class II pMHC molecule I-E^k complexed with the moth cytochrome C peptide MCC 88-103 (MCC–I-E^k)[6]. Over approximately 10 min, TCR microclusters, together with bound pMHC[4–6,9], are transported on the cell surface to the immunological synapse centre, where they are consolidated into an immobilized domain[6]. To follow ultrastructural changes associated with immunological synapse formation, TcrAND T cells were fixed after 5, 10, 15 and 20 min of interaction with supported lipid bilayers containing MCC–I-E^k and ICAM-1, and imaged first by TIRFM and then by TEM. As a control, we used the non-cognate pMHC β2m–I-E^k, which did not arrest motility or induce immunological synapse formation in TcrAND T cells (Supplementary Fig. 2a). TEM time series of TcrAND T cells forming immunological synapses on antigen-containing bilayers revealed changes in cell morphology that were characteristic of antigen-induced cell polarization (Supplementary Fig. 2b–d). Notably, at the 10 min time point, the centre of the T-cell contact interface showed an unexpected change in morphology, from a planar plasma membrane in continuous close apposition with the planar bilayer (Fig. 1a) to the appearance of numerous microvesicles (Fig. 1b and Supplementary Fig. 2e), approximately 70 nm in diameter (Supplementary Fig. 3a), that were contained within a central extracellular cavity (Fig. 1b). Microvesicle formation was antigen-specific, as they did not form with bilayers containing β_2m–I-E^k (Fig. 1a and Supplementary Fig. 2e), and could be modulated by the potency of the activating ligand, or by provision of costimulation[10] (Fig. 1f and Supplementary Discussion). To visualize the distribution of microvesicles more clearly and verify their dissociation from the plasma membrane, we performed dual-axis tomography (Supplementary Video 1) on four serial sections through an immunological synapse, ranging from 150–250 nm in thickness. The associated three-dimensional model (Fig. 1c–e and Supplementary Videos 2 and 3) of the joined tomograms demonstrated that discrete extracellular microvesicles, with no connection to overlying plasma membrane (Supplementary Fig. 4a, b), predominate in the central cavity, along with occasional membrane projections and membrane buds of nascent microvesicles (Supplementary Fig. 4c–i).

Comparison of the distributions of TCRs and microvesicles at the immunological synapse demonstrated that they were spatially correlated (Supplementary Fig. 3b–d). To establish whether TCRs present at the immunological synapse centre were associated with microvesicles, we developed a novel method for optical–electron microscopy correlation, based on registration of TIRFM and corresponding TEM images of immunological synapses aligned using a microfabricated grid (Supplementary Fig. 5). Electron tomography of T-cell–bilayer interfaces confirmed the presence of microvesicles within a roughly circular extracellular cavity at the immunological synapse centre (Fig. 1h, i and Supplementary Videos 4 and 5). Optical–electron microscopy correlation

[1]Program in Molecular Pathogenesis, Helen L. and Martin S. Kimmel Center for Biology and Medicine of the Skirball Institute of Biomolecular Medicine, 540 First Avenue, New York, New York 10016, USA. [2]Program in Structural Biology, Helen L. and Martin S. Kimmel Center for Biology and Medicine of the Skirball Institute of Biomolecular Medicine, 540 First Avenue, New York, New York 10016, USA. [3]Northwestern University Atomic and Nanoscale Characterization Experimental Center, Northwestern University, 2220 Campus Drive, Evanston, Illinois 60208, USA. [4]Department of Biomedical Engineering, Columbia University, 500 W 120th Street, New York, New York 10027, USA. [5]Department of Cancer Immunology and AIDS, Dana-Farber Cancer Institute, 450 Brookline Avenue, Boston, Massachusetts 02215, USA. [6]Program in Immunology, Harvard Medical School, Boston, Massachusetts 02215, USA. [7]New York Structural Biology Center, 89 Convent Avenue, New York, New York 10027, USA. [8]Department of Pathology, New York University School of Medicine, 540 First Avenue, New York, New York 10016, USA. [9]Kennedy Institute of Rheumatology, Nuffield Department of Orthopaedics, Rheumatology and Musculoskeletal Sciences, The University of Oxford, Roosevelt Drive, Headington, Oxford OX3 7FY, UK.
*These authors contributed equally to this work.

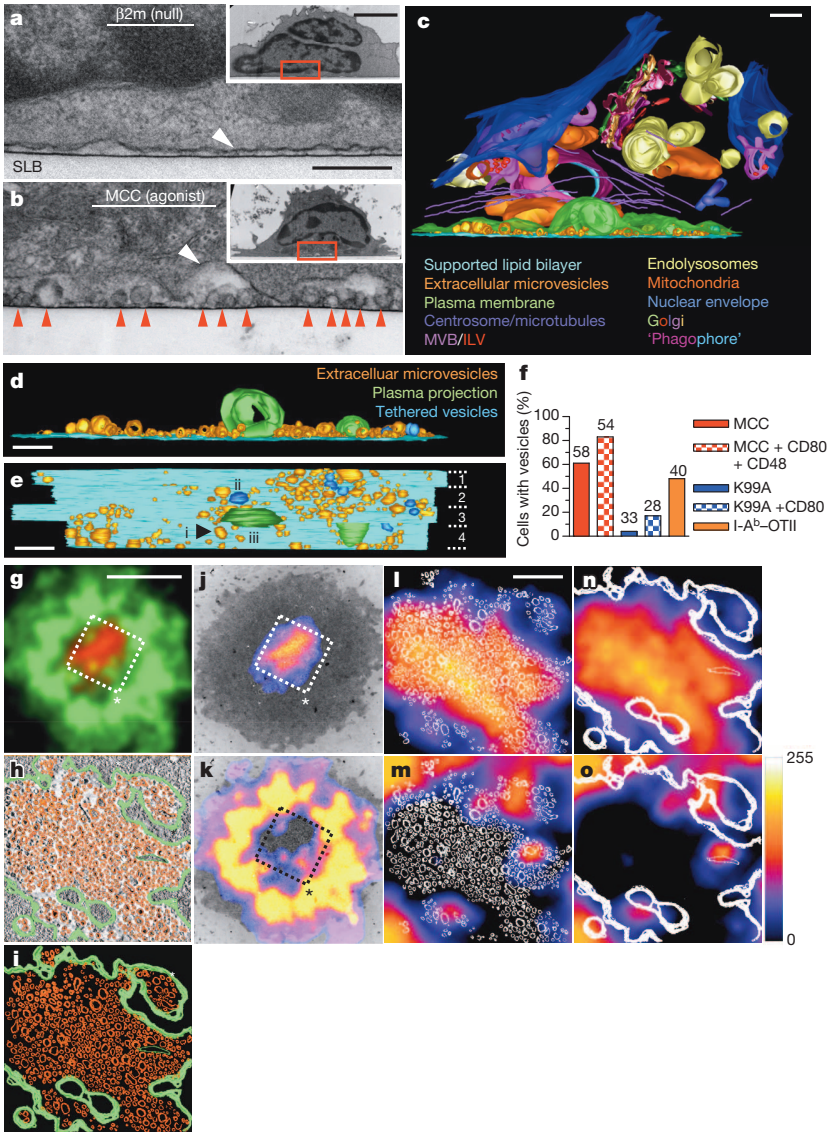

Figure 1 | Antigen-induced release of TCR-enriched microvesicles at the centre of immunological synapse. **a**, **b**, Transmission electron micrographs of TcrAND T cells interacting with supported lipid bilayers (SLB) containing ICAM-1, and the indicated pMHC. Inset, low magnification images of the same cells. Scale bar, 500 nm; inset scale bar, 2 μm; red arrowheads, extracellular microvesicles; white arrowheads, plasma membrane. **c**, A three-dimensional ultrastructural model of the immunological synapse centre. The model was constructed from dual-axis tomograms of four serial sections made orthogonal to the bilayer from a single immunological synapse (numbered in **e**). ILV, intraluminal vesicle; MVB, multivesicular body; scale bar, 250 nm. **d**, Model from **c** with intracellular components and plasma membrane removed. Scale bar, 250 nm. **e**, Model from **d** rotated 90° in the *x* axis. Examples of an extracellular microvesicle (i), tethered vesicle (ii) and plasma membrane projection (iii) are indicated. Dotted lines, section boundaries; scale bar, 250 nm. **f**, Quantification of microvesicle production by TcrAND T cells in response to MCC–I-E^k (100 molecules per μm^2) or the weak agonist K99A–I-E^k (100 molecules per μm^2), or with additional co-stimulation provided by CD80 and CD48 on bilayers (200 molecules per μm^2 for both). Microvesicle production by OTII T cells, in response to ovalbumin–I-A^b pMHC ligand (100 molecules per μm^2), was also measured. *n* is indicated above bars. Results are pooled from two independent experiments. **g**–**o**, Optical-electron tomography correlation. **g**, Overlay of TCR (red) and F-actin (green) fluorescence in TIRFM images of the TcrAND T cell immunological synapse. Scale bar, 3 μm, which also applies to **j** and **k**. **h**, A three-dimensional model of the immunological synapse centre constructed from an electron tomogram taken parallel to the T-cell–bilayer interface in **g**. T-cell plasma membrane, green; microvesicles, orange. The model is overlaid on a slice of the tomogram, and shown separately in **i** (scale bar in **l**, 500 nm, which also applies to **h**, **i** and **m**–**o**). **j**, **k**, Overlay of TCR (**j**) and F-actin (**k**) fluorescence from **g**, shown as a heat map, with the electron micrograph of the same T-cell–bilayer interface. Dashed boxes and asterisk in **g**, **j** and **k** indicate the orientation of the immunological synapse in relation to the tomogram and model overlays in **h**, **i** and **l**–**o**. **l**, **m**, Overlay of microvesicles modelled in **i** (white), scaled and aligned with the TCR fluorescence in **j** (**l**) and F-actin in **k** (**m**). **n**, **o**, Overlay of the T cell plasma membrane is modelled in **i** (white) scaled and aligned with the TCR fluorescence from **j** (**n**) and F-actin from **k** (**o**).

then allowed us to assign molecular distributions to immunological synapse ultrastructure. This revealed that TCR fluorescence at the immunological synapse (Fig. 1g, j) corresponded almost exclusively to extracellular microvesicles contained within the cavity at the immunological synapse centre (Fig. 1l, n). The characteristic F-actin depletion at the immunological synapse centre[11] (Fig. 1g, k) is also circumscribed by the plasma membrane boundary of the central cavity (Fig. 1o), reflecting interruption of cytoplasmic continuity at the immunological synapse centre. The annular ICAM-1–LFA-1 adhesive domain, which surrounds centrally accumulated TCRs (and associated MCC–I-E^k), is wholly contained within the plasma membrane border of the central cavity (Supplementary Fig. 6), which effectively precludes membrane-tethered LFA-1 from binding ICAM-1 at the immunological synapse centre. Our finding that TCRs are present in extracellular microvesicles also accounts

for the inability of centrally accumulated TCRs to exchange with TCRs elsewhere in the T cell (Supplementary Fig. 1a, b), and for the confined cytoplasmic diffusion observed at the immunological synapse centre (Supplementary Fig. 1c).

After 30–45 min, TcrAND T cells break immunological synapse symmetry and resume motility[12]. Migrating T cells left behind 80% of TCRs in particles on the bilayer (Supplementary Figs 7a, c and 8a and Supplementary Video 6). Optical–electron microscopy correlation of TcrAND T cells resuming motility after immunological synapse formation confirmed that these particles were extracellular TCR-enriched microvesicles released from the immunological synapse centre (Fig. 2a, b). The microvesicles diffused apart, which allowed us to characterize their composition by indirect immunofluorescence labelling and TIRFM (Supplementary Fig. 8b). TCR-enriched microvesicles were devoid of tyrosine phosphorylation (Fig. 2c), consistent with termination of TCR signalling. TCR-enriched microvesicles clustered MCC–I-E^k, but not β2m–I-E^k, on bilayers (Fig. 2d and Supplementary Figs 7d and 9), establishing that TCRs were on the external surface of microvesicles and were capable of binding cognate pMHC.

To investigate the mechanism by which microvesicles were produced, we next studied the role of the endosomal sorting complex required for transport (ESCRT)-I member TSG101, which was previously implicated in ubiquitin-dependent sorting of TCRs to the immunological synapse centre[6]. ESCRT-I proteins, such as TSG101, typically carry out the first in a series of steps leading to vesicle budding and fission[13]. We suppressed TSG101 expression in TcrAND T cells with small interfering RNA (siRNA), and treated cells with non-targeting small oligo-RNA (sRNA) as a control (Supplementary Fig. 10a). As expected, TcrAND T cells, in which TSG101 expression was suppressed, failed to translocate TCRs, together with bound MCC–I-E^k, to the immunological synapse centre, whereas central TCR accumulation was unaffected by treatment with control sRNA (Supplementary Fig. 10b, c). Optical–electron microscopy correlation revealed that suppression of TSG101 resulted in accumulation of TCRs, together with bound MCC–I-E^k, in a ring around the central cavity defining the immunological synapse centre (Fig. 3a), whereas treatment with control sRNA had no effect on TCR incorporation into microvesicles (Supplementary Fig. 10d). Suppression of TSG101 reduced, but did not abolish, microvesicle production (Supplementary Fig. 11). Notably, the remaining microvesicles present at the immunological synapse centre were devoid of TCRs, demonstrating that TSG101 was necessary for sorting of TCRs into microvesicles (Fig. 3a).

We next investigated the role of the ESCRT-III complex, which is responsible for the final steps in vesicle fission. We used primary human

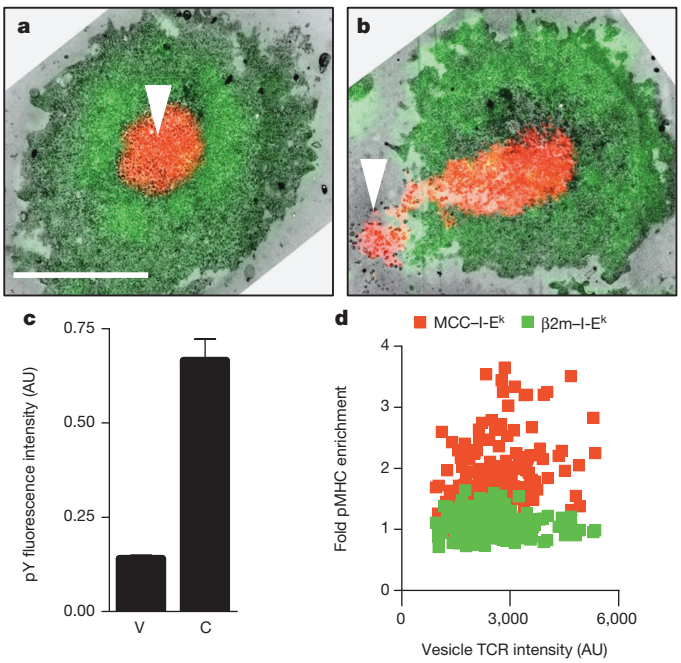

Figure 2 | TCR-enriched microvesicles are post-signalling extracellular products of T-cell activation that retain pMHC-binding competence. **a**, **b**, Optical–electron microscopy correlation of sessile TcrAND T cells forming an immunological synapse in response to MCC–I-E^k and ICAM-1 (**a**) and resuming motility (**b**), showing the distributions of F-actin (green) and TCRs (red) in relation to released microvesicles deposited on the bilayer (arrowheads). Scale bar, 4 μm. **c**, Quantification of phosphotyrosine (pY) fluorescence intensity in arbitrary units (AU) of released TCR-enriched microvesicles (V) and their originating cells (C) detected by indirect immunofluorescence labelling and TIRFM. **d**, Enrichment of fluorescently labelled cognate MCC–I-E^k or non-binding β2m–I-E^k by released TCR-enriched microvesicles. Fold pMHC enrichment is defined as: (pMHC fluorescence intensity colocalized with TCR-enriched microvesicles)/(free bilayer pMHC fluorescence intensity). Error bars represent s.e.m.

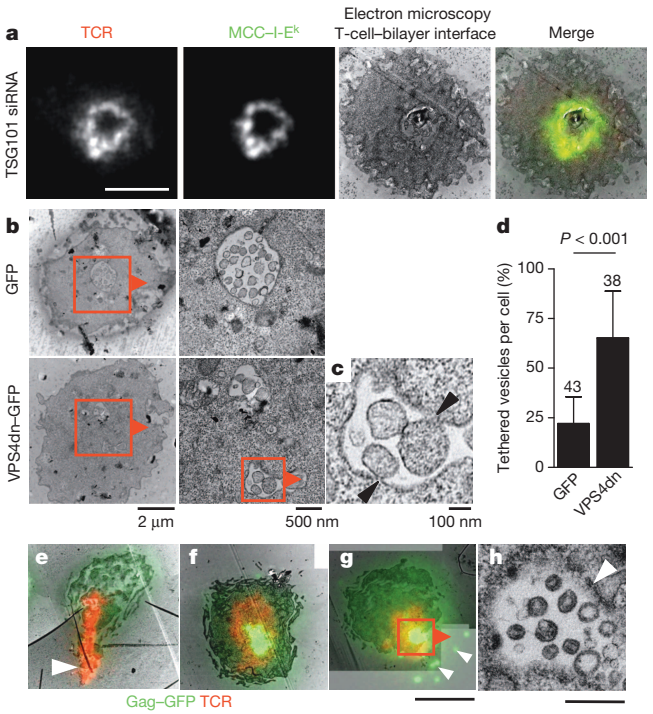

Figure 3 | Biogenesis of TCR-enriched microvesicles is mediated by ESCRT proteins and antagonized by HIV Gag. **a**, Optical–electron microscopy correlation of TCR and MCC–I-E^k distributions of a representative TcrAND T cell following siRNA-mediated TSG101 suppression. Scale bar, 3 μm. **b**, Electron micrographs of the T-cell–bilayer interface of human CD4$^+$ T cells forming an immunological synapse in response to TCR engagement. Cells were transfected with a construct encoding dominant-negative VPS4 fused to GFP (VPS4dn–GFP) or GFP only. Red boxes and arrowheads indicate regions imaged at higher magnification in panels on the right. Arrowheads in **c** indicate nascent vesicles tethered to the plasma membrane. **d**, Quantification of limiting membrane-tethered microvesicles expressed as a percentage of total microvesicles within central compartments of the immunological synapse in cells expressing indicated constructs. Means and s.d. are shown, *P* value is for Student's *t*-test. *n* is indicated above data bars. Results are pooled from two independent experiments. **e**–**g**, Representative optical–electron microscopy correlation of the immunological synapse in human CD4$^+$ T cells transfected with a construct encoding HIV Gag fused to GFP (Gag–GFP, green). Red, TCR; scale bar, 3 μm. **e**, T cell without central Gag–GFP accumulation resuming migration and releasing TCR-enriched microvesicles (arrowhead). **f**, T cell forming an immunological synapse with centrally accumulated Gag–GFP. **g**, T cell with centrally accumulated Gag–GFP resuming motility and releasing Gag–GFP-containing microvesicles (arrowheads). **h**, Higher magnification image of boxed region in **g** showing internal juxta-membrane density in Gag-containing microvesicles. Arrowhead, plasma membrane; scale bar, 500 nm.

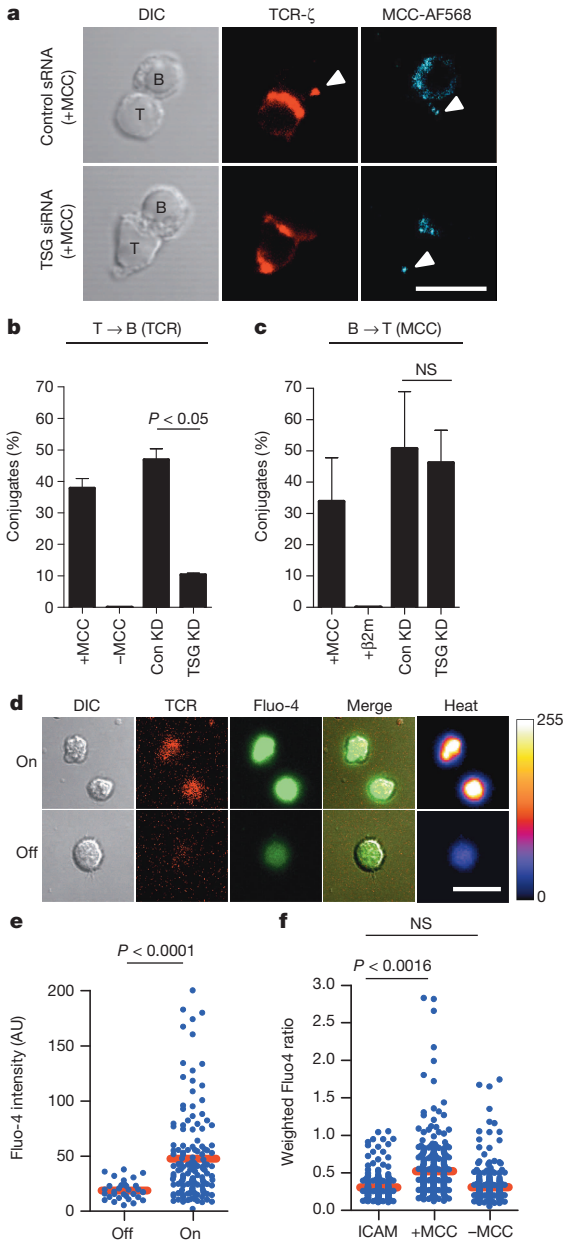

Figure 4 | TSG101 selectively controls TCR transfer to B cells that signal in response to pMHC engagement by microvesicle-tethered TCRs. **a**, Confocal microscopy of TcrAND T cells, treated with TSG101 suppressing siRNA (TSG siRNA) or control oligo-RNA (Control sRNA), forming conjugates with congenic splenic B cells loaded with fluorescent MCC peptide (cyan). $T = 30$ min.; red, TCR-ζ; arrowheads, transferred TCR and fluorescent MCC peptide; scale bar, 10 μm. **b**. Quantification of TCR transfer to B cells in T–B conjugates. **c**. Quantification of MCC peptide transfer to T cells in T–B conjugates. NS, not significant. Means from three independent experiments are shown in **b**, **c**. Error bars represent s.d. β2m, non-stimulating control peptide. Con KD, control sRNA; TSG KD, knockdown with TSG101 siRNA. **d**, Live B cells loaded with calcium-sensitive fluorescent dye Fluo-4 were imaged by confocal microscopy on bilayers containing deposited TCR-enriched microvesicles ($T = 30$ min). Panels show differential interference contrast (DIC) and fluorescence images of TCR-enriched microvesicle patches on bilayers (red) and Fluo-4 fluorescence in B cells (green and heat map). Shown are examples of B cells interacting with TCR-enriched microvesicles (On), or on bilayer areas without detectable TCR-enriched microvesicles (Off). Scale bar, 10 μm. **e**, Quantification of Fluo-4 fluorescence intensity of B cells 'On' or 'Off' TCR-enriched microvesicles. Data are representative of two experiments. **f**, Quantification of Fluo-4 intensity of B cells pulsed with MCC peptide or without antigen, after 30 min incubation on bilayers containing ICAM-1 alone, or with bilayers containing deposited TCR-enriched microvesicles. Fluorescence values were divided by the mean Fluo-4 intensity of B cells treated with 1 μM ionomycin at the end of the experiment. Data pooled from two independent experiments. Blue dots, fluorescence intensity in individual cells; red bars, sample mean; *P* value, one-way analysis of variance corrected for all comparisons.

$CD4^+$ T cells which, like TcrAND murine T cells, produce TCR-enriched microvesicles at the immunological synapse centre (Supplementary Fig. 12). We transfected human $CD4^+$ T cells with a construct encoding a dominant-negative mutant of human VPS4(E228Q), that prevents ATP binding, fused to green fluorescent protein (VPS4dn–GFP)[13]. Expression of VPS4dn–GFP disrupts the function of endogenous VPS4[13], which binds to and catalytically disassembles[14] membrane-associated ESCRT-III oligomers and is thought to be obligatory for sustaining membrane budding reactions[15,16]. As a control, we transfected human $CD4^+$ T cells with a construct encoding GFP alone. Control T cells formed microvesicles at the immunological synapse centre, the majority of which were separated from the limiting plasma membrane of the central cavity (Fig. 3b, d). In marked contrast, the immunological synapse of VPS4dn–GFP-transfected T cells contained nascent microvesicles, within a fragmented central compartment, which remained tethered to the limiting plasma membrane (Fig. 3b–d) at constricted bud necks (Fig. 3c). Consistent with the role of VPS4 'downstream' of early acting ESCRTs, VPS4dn–GFP did not affect TCR sorting to the immunological synapse centre (Supplementary Fig. 13), although its distribution at the immunological synapse was altered when compared to wild-type VPS4 (Supplementary Fig. 14). These observations indicate that VPS4 is involved in fission of TCR-rich membrane buds, thereby producing TCR-enriched microvesicles at the immunological synapse centre[13,17].

The ESCRT pathway is also exploited by the human immunodeficiency virus (HIV) structural polyprotein Gag[8,13] for membrane budding and release of virus particles from the plasma membrane of infected cells. This prompted us to test whether Gag might interfere with the biogenesis of TCR-enriched microvesicles in human $CD4^+$ T cells. We expressed a construct encoding Gag fused to GFP (Gag–GFP) in primary human $CD4^+$ T cells, and analysed immunological synapse formation by optical–electron microscopy correlation. Transfected T cells adhered poorly to supported bilayers containing ICAM-1 alone, with small Gag–GFP puncta present throughout the contact interface (Supplementary Fig. 15b, c). Notably, TCR engagement led to robust recruitment of Gag–GFP to the contact interface (Supplementary Fig. 15b, c), where it accumulated at the immunological synapse centre, displaced TCRs (Fig. 3f and Supplementary Fig. 15d, e), and resulted in the release of Gag–GFP-containing microvesicles, which are analogous to virus-like particles (VLP) that are produced during HIV infection (Fig. 3g, h and Supplementary Fig. 15f, g). Conversely, in T cells with low Gag–GFP expression, TCRs accumulated normally at the immunological synapse centre (Supplementary Fig. 15d, e), resulting in the release of TCR-enriched microvesicles (Fig. 3e and Supplementary Fig. 15f, g). The ESCRT-binding domain of Gag is required for its recruitment and central accumulation at the immunological synapse following TCR engagement (Supplementary Fig. 16 and Supplementary Discussion). Taken together, these findings indicate that Gag antagonizes ESCRT-dependent sorting of TCRs into microvesicles, and in this context TCR ligation directs the polarized budding of VLPs at the centre of the immunological synapse.

To verify that microvesicles have a physiological role in cellular interactions, we next asked whether TcrAND T cells produce TCR-enriched microvesicles in conjugates with antigen-bearing B cells. As expected, TcrAND T cells readily accumulated TCRs at the immunological synapse centre in conjugates with MCC-pulsed congenic B10.Br B cells (Supplementary Fig. 17a, b). In approximately 40% of T–B cell conjugates (Fig. 4a, b), small puncta of TCRs could be detected in B cells 'distal' to the immunological synapse, consistent with T cell to B cell synaptic transfer of TCR-containing microvesicles, whereas no T-cell polarization or TCR transfer was detected in conjugated B cells pulsed with

β2m peptide (Supplementary Fig. 17a, b). Because TSG101 is critical for the production of TCR-enriched microvesicles in the planar bilayer model, we next investigated whether TCR transfer to live B cells is affected by siRNA-mediated suppression of TSG101[6]. In conjugates of TSG101-suppressed TcrAND T cells and MCC-pulsed B cells, transfer of TCRs was reduced by approximately 80% (Fig. 4a, b), relative to conjugates treated with control sRNA, despite effective TCR polarization to the immunological synapse (Supplementary Fig. 17b). As previously described, transfer of pMHC from B cells to T cells was also observed (Fig. 4a, c and Supplementary Fig. 17a)[18,19]. However, this pMHC transfer was unaffected by TSG101 silencing in the T cell (Fig. 4a, c), demonstrating that TSG101 selectively controls TCR transfer to B cells during bidirectional membrane exchange in T–B cell conjugates[19].

We next asked whether isolated microvesicles induce signalling in antigen-presenting B cells. Engagement of MHC II molecules on B cells triggers tyrosine phosphorylation and intracellular calcium signalling, by coupling to the B-cell antigen receptor signalling machinery[20], resulting in cell proliferation in primed B cells[21]. We therefore asked whether B cells presenting cognate MCC–I-E^k complexes are activated by specific TCRs present on microvesicles. We introduced B cells, loaded with the Ca^{2+}-sensitive dye Fluo-4, onto bilayers containing TCR-enriched microvesicles, from which T cells had been removed (Supplementary Fig. 17c), and monitored Ca^{2+} signalling by confocal microscopy (Fig. 4d and Supplementary Fig. 17d). B cells pulsed with MCC were motile on bilayers, but stopped and showed sustained increase in intracellular Ca^{2+} on encountering TCR-enriched microvesicle patches on bilayers (Fig. 4d, e). In contrast, B cells not loaded with MCC did not show an increase in Ca^{2+} relative to controls (that is, cells on bilayers with ICAM-1 alone, Fig. 4d, f). Thus, B-cell signalling by pMHC is initiated by cognate recognition of TCRs on microvesicles. In support of a role for TCR-enriched microvesicles during human T–B cell interaction, we found that Raji B cells, in superantigen-induced conjugates with human $CD4^+$ T cells[22], received TCR puncta that activate phospholipase Cγ1 (PLCγ1), a key mediator of intracellular Ca^{2+} signalling[23] (Supplementary Fig. 18).

Our finding that the immunological synapse centre is an extracellular cavity, filled with TCR-enriched microvesicles by an ESCRT-dependent mechanism, provides a fundamentally new model for supramolecular domain organization at the immunological synapse (Supplementary Fig. 19a). Shedding of TCRs in microvesicles constitutes a novel mechanism for TCR 'downregulation', following engagement by pMHC, that acts in parallel with receptor internalization[24]. Our observations raise the possibility that other immune cells known to accumulate immunoreceptors at the synapse centre, such as B[25] and NK[26] cells, may also release them in microvesicles for intercellular communication. Cognate recognition of TCR-enriched microvesicles by pMHC on B cells may provide 'help' to B cells that is calibrated to the pMHC density present on their surface, pointing to a plausible mechanism for avidity-adjusted delivery of T-cell help to B cells[27]. Finally, we find that TCR-enriched microvesicle biogenesis is a native pathway in T cells, triggered by antigen recognition, that may be co-opted by HIV proteins for polarized retroviral transmission at antigen-dependent immunological synapses (Supplementary Fig. 19b).

METHODS SUMMARY

Murine TcrAND T cells were expanded with MCC peptide and IL-2, and used once quiescent. Human $CD4^+$ T cells were isolated from peripheral blood by negative selection and used within 48 h. T cells clones were expanded for one cycle using heterologous irradiated peripheral blood mononuclear cells (PBMCs), phytohaemagglutinin (PHA) and IL-2 and used once quiescent. 1,2 dioleoyl-*sn*-glycero-3-phosphatidylcholine (DOPC) lipid bilayers containing 12.5 mol% 1,2-dioleoyl-*sn*-glycero-3-[(*N*-(5-amino-1-carboxypentyl)iminodiacetic acid)succinyl] (nickel salt) (DGS-NTA-Ni) were deposited on coverslips that were cleaned with peroxidated sulphuric acid and rinsed with pure water. Bilayers contained 100 molecules per μm^2 MCC–I-E^k, and 200 molecules per μm^2 ICAM-1 unless otherwise stated. Optical imaging was performed using a Nikon TIRF microscope and an LSM510 confocal microscope. TEM imaging and tomography was performed using Phillips CM12, CM200 and FEI Technai F20 microscopes. For optical–electron microscopy correlation, lipid bilayers were formed on coverslips containing chrome registration grids on which cells were deposited and fixed for imaging. Following TIRFM imaging of the entire grid, samples were embedded in Epon, and sectioned parallel to the bilayer. TEM images of the first parallel section contained the chrome grid imprint, allowing location, imaging and alignment of electron micrographs and tomograms with TIRFM images. Cells were transfected with DNA or RNA by nucleofection (Amaxa).

Online Content Any additional Methods, Extended Data display items and Source Data are available in the online version of the paper; references unique to these sections appear only in the online paper.

Received 27 August 2012; accepted 12 December 2013.
Published online 2 February 2014.

1. Lanzavecchia, A. Antigen-specific interaction between T and B cells. *Nature* **314,** 537–539 (1985).
2. Monks, C. R. F., Freiberg, B. A., Kupfer, H., Sciaky, N. & Kupfer, A. Three-dimensional segregation of supramolecular activation clusters in T cells. *Nature* **395,** 82–86 (1998).
3. Stinchcombe, J. C., Majorovits, E., Bossi, G., Fuller, S. & Griffiths, G. M. Centrosome polarization delivers secretory granules to the immunological synapse. *Nature* **443,** 462–465 (2006).
4. Grakoui, A. *et al.* The immunological synapse: a molecular machine controlling T cell activation. *Science* **285,** 221–227 (1999).
5. Varma, R., Campi, G., Yokosuka, T., Saito, T. & Dustin, M. L. T cell receptor-proximal signals are sustained in peripheral microclusters and terminated in the central supramolecular activation cluster. *Immunity* **25,** 117–127 (2006).
6. Vardhana, S., Choudhuri, K., Varma, R. & Dustin, M. L. Essential role of ubiquitin and TSG101 protein in formation and function of the central supramolecular activation cluster. *Immunity* **32,** 531–540 (2010).
7. Babst, M., Wendland, B., Estepa, E. J. & Emr, S. D. The Vps4p AAA ATPase regulates membrane association of a Vps protein complex required for normal endosome function. *EMBO J.* **17,** 2982–2993 (1998).
8. von Schwedler, U. K. *et al.* The protein network of HIV budding. *Cell* **114,** 701–713 (2003).
9. Kaye, J. *et al.* Selective development of $CD4^+$ T cells in transgenic mice expressing a class II MHC-restricted antigen receptor. *Nature* **341,** 746–749 (1989).
10. Linsley, P. S. *et al.* Binding of the B cell activation antigen B7 to CD28 costimulates T cell proliferation and interleukin 2 mRNA accumulation. *J. Exp. Med.* **173,** 721–730 (1991).
11. Kaizuka, Y., Douglass, A. D., Varma, R., Dustin, M. L. & Vale, R. D. Mechanisms for segregating T cell receptor and adhesion molecules during immunological synapse formation in Jurkat T cells. *Proc. Natl Acad. Sci. USA* **104,** 20296–20301 (2007).
12. Sims, T. N. *et al.* Opposing effects of PKCtheta and WASp on symmetry breaking and relocation of the immunological synapse. *Cell* **129,** 773–785 (2007).
13. Garrus, J. E. *et al.* Tsg101 and the vacuolar protein sorting pathway are essential for HIV-1 budding. *Cell* **107,** 55–65 (2001).
14. Saksena, S., Wahlman, J., Teis, D., Johnson, A. E. & Emr, S. D. Functional reconstitution of ESCRT-III assembly and disassembly. *Cell* **136,** 97–109 (2009).
15. Wollert, T., Wunder, C., Lippincott-Schwartz, J. & Hurley, J. H. Membrane scission by the ESCRT-III complex. *Nature* **458,** 172–177 (2009).
16. Stuchell-Brereton, M. D. *et al.* ESCRT-III recognition by VPS4 ATPases. *Nature* **449,** 740–744 (2007).
17. Sachse, M., Strous, G. J. & Klumperman, J. ATPase-deficient hVPS4 impairs formation of internal endosomal vesicles and stabilizes bilayered clathrin coats on endosomal vacuoles. *J. Cell Sci.* **117,** 1699–1708 (2004).
18. Martínez-Martín, N. *et al.* T cell receptor internalization from the immunological synapse is mediated by TC21 and RhoG GTPase-dependent phagocytosis. *Immunity* **35,** 208–222 (2011).
19. He, T. *et al.* Bidirectional membrane molecule transfer between dendritic and T cells. *Biochem. Biophys. Res. Commun.* **359,** 202–208 (2007).
20. Lang, P. *et al.* TCR-induced transmembrane signaling by peptide/MHC class II via associated Ig-α/β dimers. *Science* **291,** 1537–1540 (2001).
21. Cambier, J. C. & Lehmann, K. R. Ia-mediated signal transduction leads to proliferation of primed B lymphocytes. *J. Exp. Med.* **170,** 877–886 (1989).
22. Mittelbrunn, M. *et al.* Unidirectional transfer of microRNA-loaded exosomes from T cells to antigen-presenting cells. *Nature Commun.* **2,** 282 (2011).
23. Marshall, A. J., Niiro, H., Yun, T. J. & Clark, E. A. Regulation of B-cell activation and differentiation by the phosphatidylinositol 3-kinase and phospholipase Cγ pathway. *Immunol. Rev.* **176,** 30–46 (2000).
24. Liu, H., Rhodes, M., Wiest, D. L. & Vignali, D. A. On the dynamics of TCR:CD3 complex cell surface expression and downmodulation. *Immunity* **13,** 665–675 (2000).
25. Fleire, S. J. *et al.* B cell ligand discrimination through a spreading and contraction response. *Science* **312,** 738–741 (2006).
26. Vanherberghen, B. *et al.* Human and murine inhibitory natural killer cell receptors transfer from natural killer cells to target cells. *Proc. Natl Acad. Sci. USA* **101,** 16873–16878 (2004).

27. Victora, G. D. *et al.* Germinal center dynamics revealed by multiphoton microscopy with a photoactivatable fluorescent reporter. *Cell* **143,** 592–605 (2010).

Supplementary Information is available in the online version of the paper.

Acknowledgements We thank G. Schütz for suggesting the photoactivation experiment, H. Chen for microfabrication, W. Sundquist for providing Gag–GFP, VPS4–GFP and VPS4dn–GFP constructs, P. Bieniasz for Gag–mCherry, GagΔL-mCherry, ALIX-GFP and CHMP4B–GFP constructs, the New York Structural Biology Center for electron microscopy tomography, support and instrumentation and members of the Dustin laboratory for helpful discussions and contributions of reagents. We thank J. Nance for the gift of biotinylated duramycin-linked biotin. This work was supported in part by a Cancer Research Institute fellowship and NIH grant K99AI093884 (K.C.), a Wellcome Trust Principal Research Fellowship (M.L.D.), a Kennedy Trust Senior Research Fellowship (M.L.D.) and NIH grants AI043542, AI045757, AI055037, AI088377, AI093884 and EY016586 (Nanomedicine Development Center).

Author Contributions K.C., M.L.D. and D.L.S. conceived the study, K.C. and J.L. designed and performed the experiments, E.W.R. performed sectioning, L.C.K. and J.T. designed and fabricated optical–electron microscopy reference grids, K.W.W. and S.G. made essential reagents, K.C. and M.L.D. wrote the manuscript. All authors edited the manuscript.

Author Information Reprints and permissions information is available at www.nature.com/reprints. The authors declare no competing financial interests. Readers are welcome to comment on the online version of the paper. Correspondence and requests for materials should be addressed to M.L.D. (michael.dustin@kennedy.ox.ac.uk) or D.L.S. (stokes@nyu.edu).

METHODS

Proteins, peptides and antibodies. Soluble I-E^k–2×His_6 and ICAM-1–His_{12} were expressed in insect cells (S2) and isolated by affinity and fast protein liquid chromatography (FPLC) purification as previously described[6,28]. All fluorophores for amine and maleimide coupling were purchased from Molecular Probes (Invitrogen). ICAM-1 was amine-labelled using SE-Cy5 or SE-AF405. MCC, K99A and β2m peptides were synthesized by fluorenylmethyloxycarbonyl (FMOC) chemistry and single AF488, AF633 and AF568 SE fluorophores were attached at their amino termini before side-chain deprotection, trifluoroacetic acid (TFA) cleavage from resin, and HPLC purification. Peptide labelling with fluorophores was confirmed by mass spectrometry and purity was >98%. Loading of peptides onto I-E^k–2XHis_6 was performed under acidic conditions as previously described[5], and MCC–I-E^k–2XHis_6 complexes purified by FPLC, yielding fluorophore to protein ratios of 0.7–1.1. HLA–DR4 was expressed purified, refolded *in vitro* with haemagglutinin peptide, and BirA biotinylated as previously described[29]. Fab fragments of mouse TCR-β-specific antibody H57 were produced by papain cleavage and purified by ion-exchange chromatography[5]. Fab′ fragments of human CD3ε-specific antibody UCHT1 were produced by pepsin cleavage to $F(ab')_2$ fragments, reduced with 0.5 mM β-mercaptoethanol to yield Fab′ fragments with free (cysteine) thiols at their C termini, and conjugated to biotin-maleimide (Pierce) to yield monobiotinylated Fab′ fragments. Monobiotinylated UCHT1 Fab′ fragments were labelled with SE Alexa fluorophores at f/p ratio of about 3, and used in bilayers to engage and follow engaged TCRs at the immunological synapse of human T cells[29]. Monobiotinylation of mouse CD3ε-specific antibody 2C11 was performed as previously described[30]. Mouse TCR-ζ-specific monoclonal antibody H146 was amine-labelled with SE AF633. Secondary antibodies and $F(ab')_2$ fragments, fluorescently labelled streptavidin and phalloidin (Molecular Probes, Invitrogen), rabbit polyclonal antibody to ZAP-70 and β-actin (Cell Signaling Technology), mouse monoclonal antibody 4G10 against phospho-tyrosine labelled with AF488 (Millipore), anti-TSG101 and anti-CD81 rabbit polyclonal antibodies (Santa Cruz Biotechnology) were purchased and used as per the vendor's instructions for immunofluorescent labelling and western blots. Duramycin-linked biotin, was used in conjunction with fluorescently labelled streptavidin (Invitrogen) to detect phosphatidylethanolamine, and fluorescently labelled annexin V (Invitrogen) was used to label phosphatidylserine. Secondary antibodies for infrared detection in western blots were from LI-COR Biosciences.

Mice, cells and cell purification. Mice used in this work were housed under pathogen-free conditions in the Skirball Institute Central Animal Facility in accordance with local and NIH regulations, and euthanized according to the guidelines of the Panel on Euthanasia of the American Veterinary Medical Association. TcrAND.B10 and B10.Br mice were mated, and F1 progeny used for experiments at 6–8 weeks of age[2]. Spleens and lymph nodes from F_1 TcrAND mice were macerated and, following red blood cell lysis, incubated with 3 μM MCC peptide and 50 U recombinant human IL-2 in complete OK-DMEM media to expand T cells. TcrAND $CD4^+$ T cells were purified from cultures at day 4 of culture for siRNA suppression, or day 6 for all other experiments, by negative selection using mouse $CD4^+$ T cell isolation kit II (Miltenyi Biotec) (purity was >95%). B cells were isolated from macerated spleens collected from B10.Br mice using anti-mouse CD43 and CD4 magnetic beads for negative selection (Miltenyi Biotec), yielding >98% CD19+ B cells. B cells were incubated overnight with 100 ng ml^{-1} lipopolysaccharide (Sigma) and 50 μM of the indicated peptides for T-cell conjugation and Ca^{2+} experiments. Spleens and lymph nodes from PA-GFP mice, which express a photo-activatable mutant of GFP[31] in all haematopoietic cells[27], were macerated through a 40 μm sieve, and $CD4^+$ T cells were purified from released cells by negative selection. PA-GFP $CD4^+$ T cells were incubated for 6 days in OK-DMEM media, with 50 U recombinant IL-2, in anti-mouse CD3/CD28 antibody-coated flat-bottomed microtitre plates. Human polyclonal $CD4^+$ T cells were isolated by negative selection (RosetteSep, StemCell Technologies) from peripheral blood leukapheresis fractions from healthy donors (New York Blood Center). Cell purity, as determined by anti-CD4/CD3 antibody labelling and flow cytometry was >95%. Freshly isolated polyclonal human $CD4^+$ T cells were rested overnight in complete RPMI supplemented with pyruvate, and either transfected and sorted by flow cytometry, or used directly for experiments, within 48 h of isolation. Human influenza haemagglutinin peptide-specific $CD4^+$ T cell clone HA:D7[29] was expanded for 10 days using irradiated human PBMC in complete media with 5 U ml^{-1} IL-2, 2 μg ml^{-1} PHA, 10% FBS and 1% human serum.

Plasmids, cell transfection, cell sorting and siRNA suppression. Details of human Gag–GFP, VPS4–GFP, VPS4dn–GFP[13], ALIX–GFP, CHMP4B–GFP[9], Gag–mCherry and the L-domain mutant of Gag fused to mCherry[32] have been described previously. Freshly isolated human $CD4^+$ T cells were transfected with 5–8 μg of plasmid DNA, prepared using Purelink HiPure Maxiprep kits (Invitrogen), using program U-014 of an Amaxa II nucleoporator and human T-cell nucleofection reagents (Lonza) as recommended by the manufacturer. Transfected cells were sorted for GFP expression by FACS (BD FACSAria II) using a 100-μm nozzle, fitted with a receptacle cooled to 4 °C. Sorted cells were rested for 4–8 h in complete RPMI, and used for experiments within 24 h of transfection. Methods used for siRNA-mediated TSG101 suppression in TcrAND T cells, including RNA sequences and targeting validation, are described in detail elsewhere[6]. Briefly, TcrAND $CD4^+$ T cells were purified at day 4 of expansion and nucleoporated with 200 nM of targeting siRNA or non-targeting control oligo-RNA using program X001 on an Amaxa II Nucleoporator and Nucleofection reagents for mouse T cells (Lonza). A second siRNA Nucleofection was performed after 48 h rest, and TSG101 levels in cells determined by western blot 48 h after the second Nucleofection, and used in experiments.

Supported lipid bilayers. Preparation of liposomes and planar bilayer formation are described in detail elsewhere[5,28]. Briefly, for coupling of polyhistidine tagged ICAM-1 and pMHCs, equal volumes of DOPC liposomes (0.4 mM) and liposomes containing 25 mol% Ni^{2+}-NTA-DGS and 75 mol% DOPC (0.4 mM) were mixed and deposited onto clean glass aqueducts of the FCS2 flow-chambers (Bioptechs). Lipid droplets were trapped by overlaying glass coverslips cleaned using peroxidated H_2SO_4. Chambers were flooded with supplemented HEPES buffered saline (20 mM HEPES, 140 mM NaCl, 5 mM KCl, 6 mM glucose, 1 mM CaCl, 2 mM MgCl, 1% human serum albumin (HSA), pH 7.2), subsequently referred to as HBS/HSA, and flushed to remove excess liposomes, leaving deposited DOPC bilayers containing 12.5 mol% Ni^{2+}-NTA-DGS. Bilayers were uniformly fluid as measured by photobleaching/recovery. Following blocking for 30 min with 5% casein supplemented with 100 μM $NiCl_2$, to saturate NTA sites, fluorescently labelled (or unlabelled) pMHC and ICAM-1 were incubated on bilayers for 30 min with polyhistidine-tagged proteins. Protein concentrations required to achieve desired densities on bilayers were calculated from calibration curves constructed from flow-cytometric measurements of bilayer-associated fluorescence of attached proteins on bilayers formed on glass beads, compared to reference beads containing known numbers of the appropriate fluorophore (Bangs Laboratories). For attachment of mono-biotinylated proteins and polyhistidine-tagged proteins, DOPC bilayers containing 12.5 mol% Ni^{2+}-NTA-DGS and 0.05 mol% cap biotin phosphatidylethanolamine were used. Unlabelled (Prozyme) or fluorescently labelled streptavidin (Molecular Probes) was then coupled to biotin headgroups, and following extensive washing, bilayers were incubated with biotinylated proteins at concentrations determined by bead calibration assays to measure bilayer densities of biotinylated proteins. All lipids were purchased from Avanti Polar Lipids.

Microfabrication. Metal-patterned substrates were prepared using a standard lift-off approach[33]. Coverslips were spin-coated with a layer of 25 kDa poly(methylmethacrylate) (PMMA) followed by a second layer of PMMA, and finally a charge dispersion layer of Aquasave (Mitsubishi Rayon). The PMMA resist was patterned and developed using standard electron-beam lithography processes. A thin (8 nm) layer of Cr was then deposited onto the patterned surfaces using an electron beam evaporation system. The remaining PMMA and overlying metal were then removed in acetone, leaving a pattern of 20 μm × 20 μm grids, defined by lines of 3-μm width, on the coverslip surface.

Total internal reflection fluorescence microscopy (TIRFM). A Nikon Ti microscope, controlled by Nikon Elements software was used for all TIRFM experiments. The instrument was fitted with: 100× TIRF objective, numerical aperture 1.49, Andor iXon EMCCD camera, 405 nm, 491 nm, 561 nm and 633 nm laser lines, appropriate CFP/FITC/Cy3/Cy5 emission filters, SRIC cube (IRM), a programmable mechanized stage, and infrared autofocus (Perfect Focus). Cultured T cells were incubated in OK-DMEM media without IL-2 for 2 h, washed and resuspended at a density of 10^7 cells ml^{-1} in HBS/HSA equilibrated to 37 °C, for injection into flow chambers pre-positioned on the microscope stage and equilibrated to 37 °C using a flow chamber heating adaptor. For immunofluorescent labelling, all procedures were performed in flow-cells. T cells attached to lipid bilayers were fixed with 2% paraformaldehyde (PFA) for 10 min at 37 °C and washed with PBS to remove fixative and, where necessary, permeabilized for 3 min with 0.1% saponin in PBS. Samples were washed, quenched with 50 mM glycine/PBS, and blocked for 1 h with 5% BSA/PBS, before labelling with directly labelled antibodies, or unlabelled primary antibodies and appropriate fluorescently labelled secondary antibodies or $F(ab')_2$ fragments (Molecular Probes). For optical–electron microscopy correlation, lipid bilayers were formed on grid substrates deposited on coverslips (described above), resulting in square fluid bilayer patches within grids, surrounded by a continuous bilayer. T cells on grids were fixed as above, and imaged using overlapping fields by TIRFM. Following optical mapping of grids, coverslips were processed for electron microscopy as described below.

Sample preparation and sectioning for electron microscopy. T cells on supported lipid bilayers were fixed in flow cells by injecting a solution of 1% glutaraldehyde, 3% PFA, 0.3% tannic acid in 0.1 M cacodylate buffer, pH 7.4 for 1 h at room temperature and processed for electron microscopy as previously described[12]. Flow chambers were disassembled and fixed cells on glass coverslips removed and

post-fixed with 1% osmium tetroxide in 0.1 M cacodylate buffer, pH 7.4 for 1 h at room temperature. Samples were then dehydrated in a solution series containing 25–100% ethanol, and flat-embedded by placing upturned BEEM capsules containing liquid epoxy resin (Epon) over bilayer regions of coverslips. Capsules were stabilized with weights to ensure firm contact with coverslips, and cured at 60 °C for 48 h. Capsules were detached from coverslips by immersion in liquid nitrogen, polymerized resin blocks isolated, which contained embedded T cells and underlying bilayers on the (macroscopically) flat surface previously in contact with the coverslip. Blocks were used directly for sectioning to obtain views containing the entire T-cell–bilayer interface, acquired as described below, or re-embedded in Epon to obtain cross-sectional views of the T-cell–bilayer interface, in 200 nm sections collected, using a Leica UCT ultramicrotome, orthogonal to the plane of the embedded bilayer[34]. At least three serial sections of the same cell were used to determine the plane nearest to the cell centre. To acquire sections containing the entire T-cell–bilayer interface for optical correlation, block sides were trimmed, without perturbing the block face, to a region approximately 1–2 mm^2, containing grid impressions and bilayer-attached T cells. The sample block was positioned on the ultramicrotome sample holder with the block face parallel to the knife-edge in the sectioning plane (Supplementary Fig. 5a), and the sample advanced to acquire a 50 nm section from the block surface. Sections were gathered on 200 hex-mesh thin bar copper grids (EMS).

Transmission electron microscopy (TEM). Conventional projection images were recorded on a Phillips CM12 transmission electron microscope, fitted with a Gatan 4k × 2.7k digital camera. Electron tomography data collection was performed in a system under the control of serialEM software. Dual tilt axis tomographic series (tilt angle ± 70°) were recorded at 200 kV in a Tecnai F20 electron microscope at the New York Structural Biology Center. Images were acquired with a 4,096 × 4,096 CCD camera and binned by a factor of 2 at 8.85 nm pixel size. Image alignment and tomographic reconstructions were obtained using the Protomo software package. Fiducial-free single-axis tomograms were combined using IMOD[35] and tomogram segmentation performed using the Amira software package. Models were constructed and rendered from segmented tomograms in IMOD[36]. Tomograms of serial sections were aligned manually, guided by organelle membrane boundaries and the supported planar bilayer density. Segmentation and modelling was performed using IMOD[37]. Phagophore morphology was interpreted as previously described[38].

Optical–electron microscopy correlation. Optical maps of T cells on grid bilayers acquired by TIRFM were used to screen sections containing entire grid areas by electron microscopy at low magnification. The first 50 nm section off of the face of the block that was in contact with the glass coverslip containing the T cell-bilayer interface, but not subsequent sections, retained impressions from the 8 nm deep chrome grids, enabling location of individual cells in optical maps for high magnification imaging by electron microscopy and tomography. Fluorescence images were scaled to the same pixel dimensions of high magnification electron microscopy images and converted from 14-bit to 8-bit depth, preserving the aspect ratio of images. These images were then translated and rotated to match cell contours, and overlay of aligned images yielded optical–electron microscopy correlations[39]. We observed minor cell sample shrinkage in the peripheries of the cell contact interface, likely due to fixation/dehydration of electron microscopy samples, however, membrane contours within the contact centre were very well preserved, likely due to stronger adhesion, and diminished membrane fluctuations with the bilayer substrate in this region. Tomogram models of the immunological synapse centre were similarly processed to yield optical–tomogram correlations of the same cell.

Live confocal microscopy of Ca^{2+} signalling in B cells. Imaging was performed on a Zeiss LSM 510 confocal microscope. Live cell imaging was performed in FCSII flow chambers maintained at 37 °C using a heating adaptor, within an environmental chamber equilibrated to 37 °C. For Ca^{2+} imaging, lipopolysaccharide-activated B cells (incubated with or without peptides) were incubated in neat RPMI with 4 μM Fluo-4 AM (invitrogen) for 20 min at 37 °C, washed and incubated in complete RPMI for 20 min. Cells were resuspended in warmed HBS/HSA buffer at 5×10^6 ml^{-1} and introduced into heated flow chambers for intracellular Ca^{2+} imaging using 488/515-30 BP excitation/emission filters for Fluo-4 and 546/600 LP excitation/emission filters for detecting TCRs, labelled with AF-568-conjugated H57 Fab′ fragments. Transmitted differential interference contrast images were recorded with 457 nm illumination. 8-bit images were acquired serially using a 40× oil objective, numerical aperture 1.3, at 1,024 × 1,024 pixel resolution. Flow chambers contained bilayers with ICAM-1 alone (200 molecules per μm^2), or containing isolated TCR-enriched microvesicle patches. To isolate TCR-enriched microvesicles on bilayers, TcrAND T cells were allowed to form immunological synapse on bilayers containing MCC–I-E^k (100 molecules per μm^2) and ICAM-1 (200 molecules per μm^2) for 60 min, after which T cells were removed by washing flow chambers with cold HBS/HSA, that promotes de-adhesion by inactivating integrins. After screening to ensure removal of T cells, Fluo-4 loaded B cells were introduced into flow chambers, and imaged in contiguous fields after 30 min interaction with microvesicles, to survey B cell Ca^{2+} signalling, as measured by B cell Fluo-4 fluorescence intensity, in response to TCR microvesicles. For some experiments, where imaging runs were separated by long periods, necessitating independent Fluo-4 loading of separate batches of B cells, 1 μM ionomycin was introduced in flow chambers to determine maximal Ca^{2+} levels, at the end of each imaging run. This allowed correction for differences in Fluo-4 loading, expressed as individual B cell Fluo-4 fluorescence intensities/mean ionomycin induced fluorescence intensity, resulting in weighted Fluo-4 ratios.

Confocal microscopy of T–B cell conjugates. For experiments using murine T–B conjugates, lipopolysaccharide-activated B cells (incubated with or without peptides) were mixed with equal numbers of TcrAND T cells (treated with siRNA or untreated) in warmed OK-DMEM medium, and brought into contact by centrifugation at 250*g* for 2 min. Cells were incubated at 37 °C for 30 min, following which, media was aspirated and replaced with 2% PFA to fix cells. Cells were deposited on cleaned coverslips and permeabilized, blocked and labelled as for fluorescent labelling of TIRFM samples above, with extensive washing, by 6 exchanges with PBS, between each processing step. Following immunofluorescent labelling, coverslips were mounted on glass slides using Antifade Gold (Molecular Probes) and cured in the dark at room temperature for 24 h. Images of cell conjugates were acquired with a 63× Plan-Apochromat oil objective, numerical aperture 1.4.

For experiments involving human T–B conjugates, superantigen-specific $CD4^+$ T cells were expanded from human PBMC by incubation with 100 ng ml^{-1} of the superantigen SEE (staphylococcal enterotoxin E, Toxin Technology) in complete RPMI media. Following culture at 37 °C/5% CO_2 for 5 days, $CD4^+$ T cells were isolated by negative selections (EasySep, StemCell Technologies), and expanded for a further 7–10 days with 10 U ml^{-1} recombinant IL-2 (R&D Systems). Quiescent $CD4^+$ T cells were mixed in 1:1 ratio with the human Raji B cells (ATCC CCL-86), which express HLA-DR, in the presence of 1μg ml^{-1} SEE to form superantigen induced conjugates. Cells were fixed in 3% PFA after 60 min incubation at 37 °C, permeabilized and stained with primary antibodies against TCR CD3ε (clone OKT3) and an appropriate fluorescently labelled secondary antibody. For labelling of PLCγ1 phosphorylated at tyrosine 783 (Cell Signaling Technology) in addition to TCR, all incubations and labelling were performed in media/buffers containing 0.5 mM sodium orthovanadate. For selective inhibition of SYK tyrosine kinase in Raji B cells, cell conjugates were formed by gentle centrifugation, and incubated in complete RPMI for 30 min. Culture supernatant was then replaced, without disturbing cell pellets, with media containing 200 nM SYK inhibitor V (EMD Millipore), and cells incubated for a further 30 min at 37 °C before fixing for antibody labelling. Confocal imaging was performed as for murine T–B conjugates.

Image processing. All fluorescence images were background subtracted. Measurements from TIRFM images were made at native 14-bit depth. For optical electron microscopy correlations, images were scaled and converted to 8-bit depth. Confocal images were acquired at 8-bit depth. Measurements were performed using Metamorph, ImageJ and Photoshop software. For presentation in figures, images were adjusted identically across related groups for brightness and contrast.

Statistical analysis. Linear regression, Student's *t*-test, and one-way analysis of variance (corrected for all pairwise comparisons) were performed using Prism software. *P* values < 0.05 were considered statistically significant, *P* values > 0.05 were considered not statistically significant and denoted as NS in figures. Pearson's correlation coefficient (*R*r) was calculated from corresponding interface regions from two channels in TIRFM images using ImageJ.

28. Dustin, M. L., Starr, T., Varma, R. & Thomas, V. K. Supported planar bilayers for study of the immunological synapse. *Curr. Protoc. Immunol.* Ch. 18, Unit 18.13 (2007).
29. Schubert, D. A. *et al.* Self-reactive human CD4 T cell clones form unusual immunological synapses. *J. Exp. Med.* **209,** 335–352 (2012).
30. Fleire, S. J. & Batista, F. D. Studying cell-to-cell interactions: an easy method of tethering ligands on artificial membranes. *Methods Mol. Biol.* **462,** 1–10 (2009).
31. Patterson, G. H. & Lippincott-Schwartz, J. A photoactivatable GFP for selective photolabeling of proteins and cells. *Science* **297,** 1873–1877 (2002).
32. Jouvenet, N., Bieniasz, P. D. & Simon, S. M. Imaging the biogenesis of individual HIV-1 virions in live cells. *Nature* **454,** 236–240 (2008).
33. Tsai, J., Sun, E., Gao, Y., Hone, J. C. & Kam, L. C. Non-Brownian diffusion of membrane molecules in nanopatterned supported lipid bilayers. *Nano Lett.* **8,** 425–430 (2008).
34. Milstein, O. *et al.* Nanoscale increases in CD2-CD48-mediated intermembrane spacing decrease adhesion and reorganize the immunological synapse. *J. Biol. Chem.* **283,** 34414–34422 (2008).
35. Winkler, H. & Taylor, K. A. Accurate marker-free alignment with simultaneous geometry determination and reconstruction of tilt series in electron tomography. *Ultramicroscopy* **106,** 240–254 (2006).

36. Kremer, J. R., Mastronarde, D. N. & McIntosh, J. R. Computer visualization of three-dimensional image data using IMOD. *J. Struct. Biol.* **116,** 71–76 (1996).
37. Marsh, B. J., Mastronarde, D. N., Buttle, K. F., Howell, K. E. & McIntosh, J. R. Organellar relationships in the Golgi region of the pancreatic beta cell line, HIT-T15, visualized by high resolution electron tomography. *Proc. Natl Acad. Sci. USA* **98,** 2399–2406 (2001).
38. Hayashi-Nishino, M. *et al.* A subdomain of the endoplasmic reticulum forms a cradle for autophagosome formation. *Nature Cell Biol.* **11,** 1433–1437 (2009).
39. Keene, D. R., Tufa, S. F., Lunstrum, G. P., Holden, P. & Horton, W. A. Confocal/TEM overlay microscopy: a simple method for correlating confocal and electron microscopy of cells expressing GFP/YFP fusion proteins. *Microsc. Microanal.* **14,** 342–348 (2008).